Journal of Molecular Structure 1294 (2023) 136378

Contents lists available at ScienceDirect

Journal of Molecular Structure

journal homepage: www.elsevier.com/locate/molstr

Synthesis and characterization of acidic deep eutectic solvents based on p-Toluenesulfonic acid

Kapil Mamtani [a,**], Sarah J. Stevenson [b], Petrik Galvosas [b,d], Cameron C. Weber [c,d], Mohammed.M. Farid [a], Kaveh Shahbaz [a,e,*]

[a] Department of Chemical and Materials Engineering, The University of Auckland, Auckland, New Zealand
[b] School of Chemical and Physical Sciences, Victoria University Wellington, Wellington, New Zealand
[c] School of Chemical Sciences, The University of Auckland, Auckland, New Zealand
[d] MacDiarmid Institute for Advanced Materials and Nanotechnology, Wellington, New Zealand
[e] Circular Innovations (CIRCUIT) Research Centre, The University of Auckland, Auckland 1010, New Zealand

ARTICLE INFO

Keywords:
Deep eutectic solvents
Hammett acidity
Catalysts
Self-diffusion coefficient

ABSTRACT

There is growing interest in identifying suitable, less hazardous deep eutectic solvent (DES) alternatives for conventional solvents and catalysts, particularly acid catalysts which can be volatile and highly corrosive. In this study, novel acidic DESs based on mixtures of either tetrabutylammonium hydrogensulfate (TBAHS) (DES1) or tetraphenylphosphonium bromide (TPPB) (DES2) with p-toluenesulfonic acid monohydrate (PTSAM) are prepared. The properties of these DESs were investigated using multiple analytical techniques, including density, viscosity, conductivity and diffusion measurements. DES1 formed a room-temperature liquid, whereas DES2 melted at 337 K at its eutectic point. Hammett acidity studies revealed that both the DESs show super acidity (H_{0DES1} = -2.91 and H_{0DES2} = -1.89) even when present in relatively dilute (40 mM) aqueous solutions. Conductivity measurements established that both DESs show good ionicity at elevated temperatures based on a Walden plot, although DES2 displayed reduced ionicity close to its melting point. Equilibrium structural arrangements for these DESs are proposed based on findings, with the formation of a complex hydrogen-bonded anion and isolated cation. These DESs are proposed as potential replacements for ionic liquids, and existing acid catalysts in acid catalyzed reactions.

1. Introduction

Deep eutectic solvents (DESs) have recently gained recognition as potential environmentally friendly alternative solvents. DESs are typically prepared by creating mixtures containing a suitable molar ratio of hydrogen bond acceptors (HBAs) and donors (HBDs), with hydrogen-bonding interactions between these leading to a suppression of the melting point of the mixture [1]. The green properties of many DESs include their non-volatility, non-flammability, biodegradability, biocompatibility, and ability to be prepared inexpensively and energy efficiently. Due to these advantages, previous decades have seen a rise in the applications of DESs in diverse research fields such as extraction, electropolishing, corrosion inhibition/ removal, galvanization, and analytical chemistry, among other areas. Emerging alongside this is interest in the use of DES as catalysts for various chemical reactions, particularly acid-catalyzed reactions, an area where ionic liquids have been extensively investigated [1–4].

For DESs containing organic molecules, the HBAs that are commonly used are salts such as choline chloride, with HBDs consisting of urea or molecules containing functional groups such as alcohols and carboxylic acids [5,6]. Salts containing heteroatoms other than nitrogen have also been explored, with the first phosphonium-based DES described by Kareem et al. in 2010 [7]. Though less researched than ammonium-based DES, several different phosphonium-based DESs have been prepared [8–12]. These can have beneficial properties compared to ammonium-based salts, such as greater thermal and chemical stability and varied polarity of the subsequent DESs. A DES based on allyltriphenylphosphonium bromide (ATPPB) and p-toluenesulfonic acid (PTSA) (1:3) was used as an acid catalyst to esterify glycerol and oleic acid [10]. This DES procedure was subsequently used with minor

* Corresponding author at: Chemical and Materials Engineering Department, The University of Auckland 1010, New Zealand.
** Corresponding author.
E-mail addresses: kmam238@aucklanduni.ac.nz (K. Mamtani), k.shahbaz@auckland.ac.nz (K. Shahbaz).

https://doi.org/10.1016/j.molstruc.2023.136378
Received 25 June 2023; Received in revised form 3 August 2023; Accepted 6 August 2023
Available online 7 August 2023

modifications to esterify glycerol with a mixture of free fatty acids [12, 13]. Additionally, choline chloride-based DESs were used as efficient, inexpensive catalysts for the epoxidation of soybean oil with peroxyformic acid [14]. Detailed reviews [15–18] on the application of DESs for catalytic applications in diverse chemical reactions have been published.

Given the growing interest in DESs for acid catalysis, it is essential to explore and develop novel DESs with high acidity and suitable polarity. DESs' physicochemical properties depend on the chemical structure of their individual components and the molar ratio of these constituents. Additionally, the chemical structure of the components influences how well DESs function for a given application. Both ammonium- and phosphonium-based DESs have been used for biorefinery applications as catalysts and solvents. In this work, two novel DESs are prepared based on p-toluenesulfonic acid monohydrate (PTSAM) as the HBD. These DES feature tetrabutylammonium hydrogensulfate (TBAHS, DES1) and tetraphenylphosphonium bromide (TPPB, DES2) as HBAs. Physical properties, such as density, conductivity, and viscosity, were measured at different temperatures. Investigations into the structure using vibrational spectroscopy and self-diffusion studies and Hammett acidity measurements, were also carried out. It is expected that this study will enable greater insight into these potentially useful DESs and aid in developing DESs in the field of acid catalysis.

2. Experimental

2.1. Materials

The chemical structures of the HBAs and HBD used in this study are shown in Fig. 1. All the chemicals used in this study and their supplier are listed in Table S1 in the supporting information. All purchased chemicals were used as received without additional purifications.

2.2. Preparation of deep eutectic solvents

The method of preparation of the DESs used in this work is similar to that used in previous work [12]. DESs were prepared by weighing the appropriate mass of each component in a Schott bottle, which was stirred and heated to 373.15 K for 3 h until a homogeneous liquid was obtained. TBAHS was mixed with PTSAM in a 1:2 molar ratio to prepare DES1, while TPPB was mixed with PTSAM in a 1:3 molar ratio to prepare DES2. The DESs were stored in the sealed Schott bottle, with parafilm used to help prevent the ingress of moisture.

2.3. Melting point and water content determination

Eutectic points were determined by analyzing the melting points of the DES at different compositions. Melting and freezing points were determined by differential scanning calorimetry (DSC) using a PerkinElmer DSC 8500 instrument. Approximately 15–20 mg of the sample was weighed onto an aluminum pan and introduced into the instrument. For DES1, a temperature cycle of 198.15 K to 303.15 K at 2 K/min ramp rate was applied, with an initial hold of 60 min at 198.15 K. For DES2, it was 298.15 K to 393.15 K at 5 K/min ramp rate. For the pure constituents, the upper limit of the temperature ramp was at least 20 K more than the reported melting point. The water content of the DESs was measured using Karl Fischer (KF) Moisture Analyzer (T5, Mettler Toledo). The measurement accuracy of the Karl Fisher coulometer was checked with HYDRANAL–water standard 10.00 mg/g and KF had a high accuracy and precision, typically within 1% of available water. This standard was supplied in glass ampoules from Merck Pty Limited.

2.4. FT-IR

A PerkinElmer UATR Two FT-IR instrument was used in the ATR mode for FT-IR. The data was collected with a 4 cm^{-1} resolution with 8 scans per run. Neat samples were introduced on the scanning window at room temperature for scanning.

2.5. Raman spectroscopy

Raman spectroscopy was performed using a confocal Raman microscope (Horiba LABRAM HR Evolution) equipped with an air-cooled neodymium-doped yttrium aluminum garnet (Nd-Yag) laser (excitation wavelength 532 nm) operating at 100 mW with a 50X optical microscope. Spectra were acquired with 600 grooves/mm diffraction grating, while background fluorescence was filtered using a polynomial expression. For viscous liquid phase samples, a small drop of the sample was placed on one of the KBr plates. Then the second KBr plate was placed on top of it and rotated to develop an even thin film. The arrangement of plates was then placed onto the sampling stage, and the spectrum was run. Care was taken to clean the KBr plates, and gloves were worn to prevent smudges or fogging. After running a spectrum, the two KBr plates were wiped and rinsed methylene chloride (twice), followed by ethanol.

2.6. NMR

NMR experiments to characterize the DES were performed on a Bruker AVIII400 spectrometer (^1H-NMR frequency of 400 MHz) with probe temperature of 298 K. 40 mg of each DES were dissolved in 0.5 mL of d_6-DMSO. Their respective components were analyzed at the same concentration as in the DES sample. ^1H-NMR experiments were performed using 16 scans, with chemical shifts referenced to the residual solvent signal. The instrument was suitable for NMR experiments at varying temperatures between 300 to 380 K. Neat samples, were measured around their respective melting points. MestReNova 11.0 (Mestrelab Research) application was used to process the raw NMR data.

Self-diffusion studies were performed on a Bruker Avance400 spectrometer (400 MHz ^1H frequency) equipped with a Bruker Diff60 diffusion probe. The maximum gradient strength used was 3.6 T/m in the z-direction. Diffusion experiments were performed between 343 – 423 K for DES1 and 363–403 K for DES2, with 20 K interval steps. The actual temperature may deviate as higher temperatures are probed, up to ± 10 K. The sample temperature was equilibrated for 30 minutes using the Bruker Variable Temperature unit, BVT 3000, before analysis. 5 mm NMR tubes were used for testing. A 13-interval pulsed gradient stimulated echo sequence (PGSTE) with bipolar sinusoidal shaped

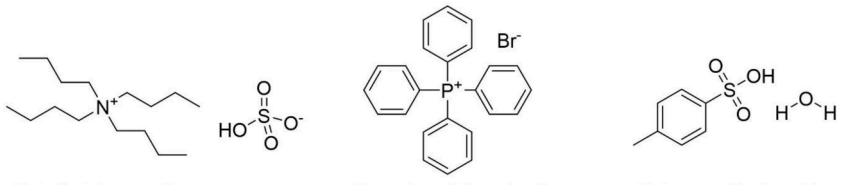

Fig. 1. Chemical structures of the compounds used to prepare DESs.

gradients (Bruker name = diffSteBP) was used, with the observation time (Δ) fixed to 40 ms. The gradient pulse duration (δ) was fixed for each individual temperature step, and the gradient strength (g) was varied in 16 steps. All self-diffusion NMR data were processed via Top Spin 2.1. The error in the estimation of D_s values in plots is estimated to be 10%, primarily owing to choices in signal phasing, baseline correction and integration limits. The self-diffusion study methodology was adapted from the works of D'Agostino et al. [19].

2.7. Thermogravimetric analysis

Thermogravimetric analysis of the DESs was done on the NETZSCH STA 449F5 STA449F5A-0382-M instrument. All measurements were carried out at atmospheric pressure. Approximately 10 mg of the sample was weighed in an open aluminum pan, and the temperature increased at 10 K/min. All the samples were analysed in triplicates to ascertain measurement reliability.

2.8. Density measurements

The mass densities (ρ) of the DESs were determined using a DMA 4500 vibrating tube density/specific gravity meter (Anton Paar, Austria). To check the density meter adjustment, the density of water (degassed bi-distillated) was measured at 298.15 K. Density measurements were carried out at temperatures from 323.15 to 363.15 K at 10 K intervals. All measurements were done in triplicate at atmospheric pressure within a fume hood. While the quoted accuracy for the instrument was 0.01%, replicate experiments identified reproducibility to within 5%. This discrepancy is likely due to the viscosity, and associated sample loading issues for the solutions used. Error in the estimation of ρ values was calculated to be less than 5%.

2.9. Viscosity measurements

Dynamic viscosity (η) was measured using the AR-G2 Magnetic Bearing Rheometer (TA Instruments Ltd) with a temperature-controlled environment at a shear rate of 100 s^{-1}. The investigated temperature ranges were 323.15 K-363.15 K. The temperature range was chosen based on the melting point of the DESs and the thermal degradation range. The quoted accuracy of the sample temperature and viscosity are 0.05% and 0.1%; however, replicate values indicated that the uncertainty for these values were approximately 2% and 5%, respectively. As for the density measurements, it is likely that these larger than expected uncertainties are due to the high viscosity of these samples and associated sample loading difficulty.

2.10. Conductivity measurements

The electrical conductivity (K) of the DESs was measured at different temperatures using a Mettler Toledo Seven Compact S230 conductivity meter equipped with a 2 platinum poles conductivity cell with a chemical resistant glass body. The temperature variation was achieved by using a water bath with temperature control. For each measurement, three replicates were carried out, and the uncertainties of the electrical conductivity and temperature values were within the range of ±0.003 mS cm^{-1} and ±0.1 K, respectively.

2.11. Hammett acidity measurements

The Hammett acidity function (H_0) was calculated according to Eq. (1) following Hammett et al. [20], where "I" is the indicator, $pK(I)_{aq} = pKa = 0.99$, $[IH^+]_s$ and $[I]_s$, represents the absorbance ratios of protonated and un-protonated indicator forms.

$$H_0 = pK(I)_{aq} + \log\left(\frac{[I]_s}{[IH^+]_s}\right) \quad (1)$$

Water is used as a solvent to prepare solutions of DESs, as both DESs are soluble in water. An aqueous solution of PTSAM was also made to analyze the effect of the HBAs on the acidity of DESs. All the measurements were done by a Shimadzu UV-2550 UV Vis spectrophotometer. The typical procedure follows the work of Zhu et al. [21]. 5 mM to 40 mM aqueous solution of samples and a 0.1 mM aqueous solution of indicator dye was prepared. The sample and indicator solution were mixed in ratios from 1:0.5 to 1:2 to see the effect of indicator concentration on acidity. After mixing, the combined solution was transferred to a quartz cuvette with a 10 mm path length and the UV–Vis spectrum was obtained at 298.15 K. The maximum absorption wavelength and peak intensity wavelength were recorded and exported into Microsoft Excel for analysis. Maximum absorbance of 1.096 at 370 nm for indicator dye (0.1 mM) is observed, and this was taken as the reference for the un-protonated indicator for further calculations.

3. Results and discussion

3.1. Melting and eutectic points

It is essential to study the melting and eutectic behavior of the DESs prior to using them for various applications, as polymorphism or different metastable phases might exist. This is crucial when considering the recycling of the solvent. The eutectic point investigation was done by mixing the two components of each DES at different molar ratios and determining the melting point of each composition using DSC. The phase diagrams for both DES are shown in Fig. S1. The eutectic composition corresponds to the minimum melting point in these curves. Table 1 shows the eutectic composition and associated melting points of the studied DESs. The melting point DSC data for the both DESs is shown in Table S2 and S3, provided in the supplementary information. While the glass transition temperature for DES1 was somewhat lower at 1:2.5 molar ratio than at 1:2 molar ratio, a solid-liquid mixture was observed for the former, therefore the latter was chosen as eutectic point, where a homogeneous liquid mixture was detected.

The molecular weight of DESs is poorly defined due to the presence of the mixture, with two approaches being a weighted average approach where the average molecular weights of the constituents are used, as per the works of Ghaedi et al. [22]. or an aggregate approach where the sum of the molecular weights of all components are used (Table 1). For the measurement of physico-chemical properties relating to the number of ions (Λ_m and H_0), the aggregate approach was used as this more accurately reflects the concentration of charge carriers. Water content in both DESs is also shown in Table 1 and was less than 5%. PTSAM should account for ~5 wt.% water in both samples (5.0 and 5.5 for DES1 and DES2, respectively). This suggests that the reported water values are similar to those expected based on the reported mixtures, considering the accuracy of KF titrator lies within 1% and PTSAM was 98.5% pure. Also, slight deviations with theoretical water content may arise from sample loading and injecting issues with KF titrator. Both mixtures displayed clear evidence of the formation of eutectic mixtures due to a reduction in melting point with respect to both pure components.

The depression in melting points of these DESs is hypothesized to be due to extensive hydrogen bonding between components in the mixture, which leads to an increase in the entropy of the mixture in the liquid state [23]. The bulky structure of the HBA cation in DES1 may result in

Table 1
Eutectic composition, melting point, and water content of the studied DESs.

ID	DES	Molar ratio	Molar mass (g/mol)	Melting Point (K)	Water content (%)
DES1	TBAHS-PTSAM	1:2	719.94	229.97	4.50
DES2	TPPB-PTSAM	1:3	989.96	337.45	4.37

weak cation-anion interactions induced by these HBD-HBA anion hydrogen bonds, as well as more inefficient crystal packing, which could further account for the large depressions in melting point [24].

3.2. FT-IR

FT-IR was used to interrogate hydrogen-bonding interactions between components of the DES. Fig. 2 illustrates the FT-IR spectra of the pure salts, PTSAM and DESs. PTSAM and the salt were mixed in a molar ratio of 2:1 and 3:1 in the case of DES1 and DES2. Therefore, the relative intensities of peaks arising from PTSAM are stronger than those of the salts in the respective DES spectra.

For DES1, a very slight blue shift in the O-H stretching modes in the 3200–3500 cm^{-1} range is observed compared to pure PTSAM. This can be attributed to the presence of hydrogen bonding interactions between the PTSAM and $[HSO_4]^-$ anion in the DES, similar shifts in O-H stretching have been observed for related DESs [25,26]. For DES2, a similar but more pronounced blue shift in the O-H stretching modes are observed in the 3000–3500 cm^{-1} region between pure PTSAM and DES2. Similar to DES1, this would be consistent with hydrogen bonds formed between PTSAM and the salt, in this case, the $[Br]^-$ anion of the salt. The blue shift in O-H stretching vibrations for the two DESs suggests weak hydrogen bond interactions [27] between the respective salt and the PTSAM. This weak H-bonding network directly results from bulkier substituents in both salts [28]. Hence, the observed FT-IR spectra suggest the formation of hydrogen bonds between HBD and HBA in both DESs.

3.3. Raman spectroscopy

In Fig. 3(a) and Fig. 3(b), no considerable changes are seen in the DES spectra and the spectra of the individual components for both DES1 and DES2. This implies that even though there is hydrogen bond formation, as suggested by the IR spectroscopy, the HBA cations still interact with their counter anions, respectively, in the presence of HBD (PTSAM); a similar observation was reported by Muzio et al. [29] when characterizing quaternary ammonium-based DES.

There is a weak signal, a new peak observed at 1380 cm^{-1} in Fig. 3(a) and Fig. 3(b) for both DESs spectra. This weak signal might indicate the O-H group arising potentially from water present in the DESs [31]. This could mean more water is present in the synthesized samples than the individual components.

3.4. ^{1}H-NMR

Fig. S2 (a-e) displays the NMR spectra for individual salts, acid, DES1 and DES2. The spectra of each component TBAHS, TPPB, and PTSAM are consistent with the reported literature [32]. For DES1, all the components' peaks are present but with a slight up-field chemical shift compared to the pure components signal. This up-field shift in the DES1 implies the shielding effect due to interactions between quaternary ammonium cation with oxygen atoms of PTSAM [34]. This would be consistent with a reduction in H-bonding interactions by the cation which might be due to the PTSAM interacting with the $[HSO_4]^-$ anion. This leads to an increase in the electron-withdrawing effect of the cation and reduced electron density around H atoms. This is also consistent with the significant downfield shift of the OH of the PTSAM in DES1, indicating the formation of ion-hydrogen bond complexes [33]. For DES2, while a similar trend is observed for individual component peaks having a slight up-field chemical shift, the OH of PTSAM (6.69 ppm) moves up-field (6.16 ppm) in DES2. The explanation for this phenomenon is less clear as it would be unlikely to be due to reduced

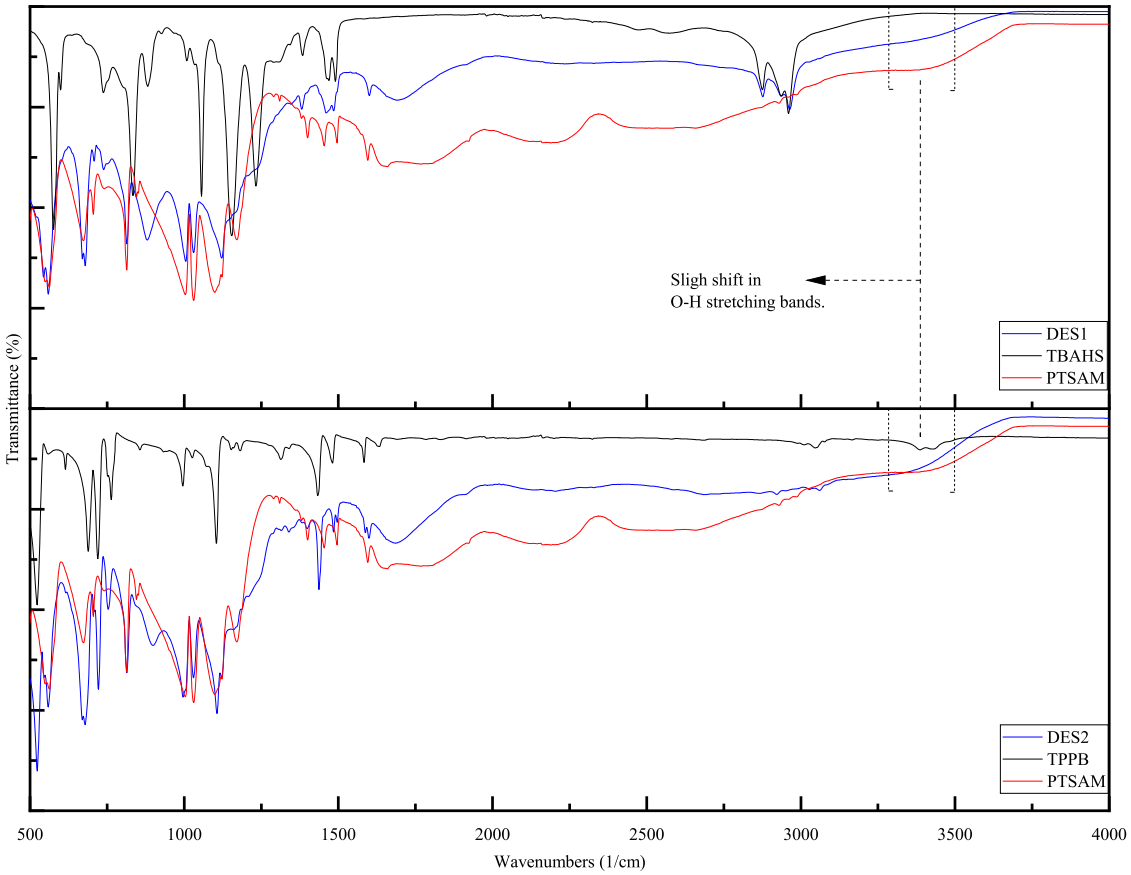

Fig. 2. FT-IR plots for the two DESs. (color).

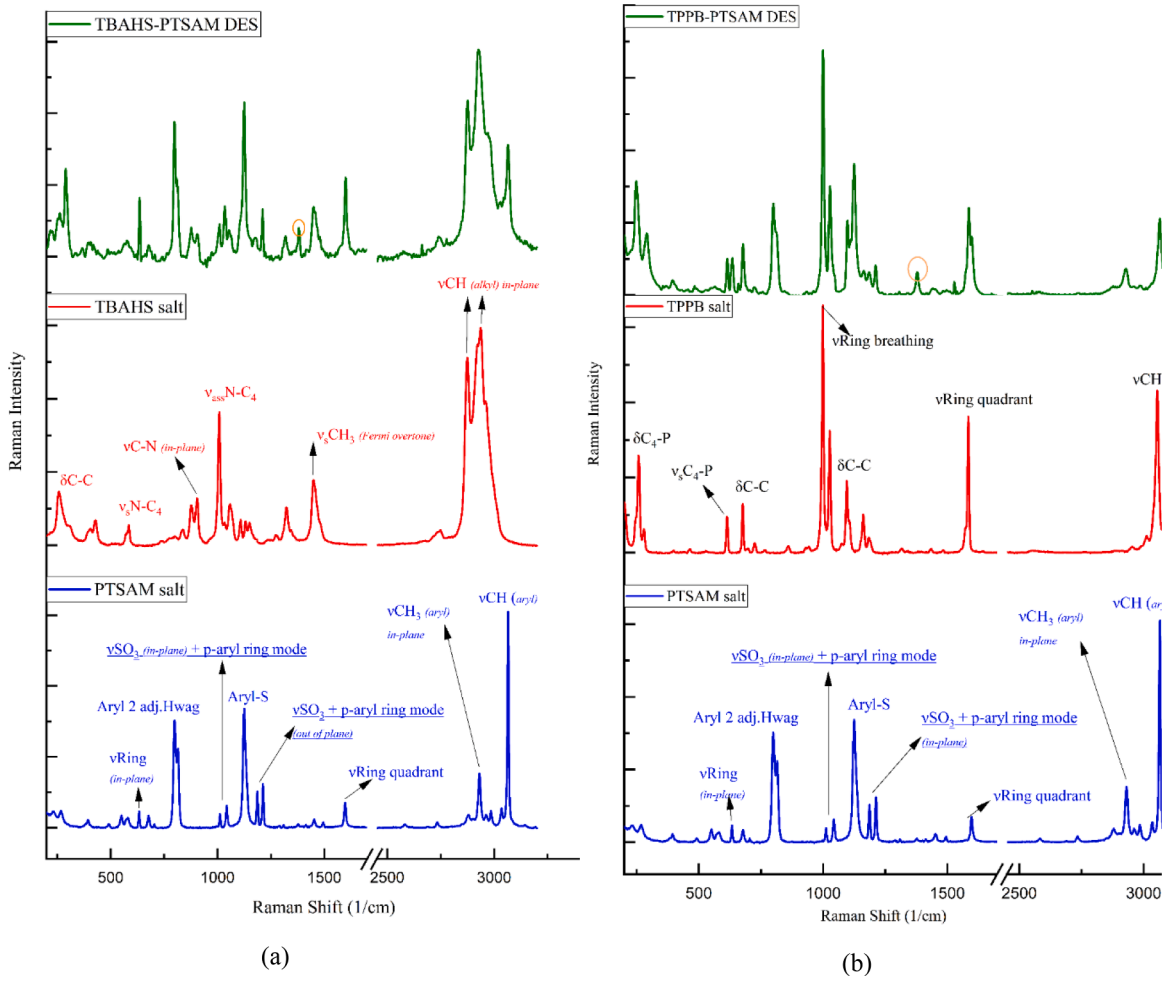

Fig. 3. Raman spectra measured for: (a) TBAHS salt (red), PTSAM salt (blue) pure components and the DES1 (1:2) (green); (b) TPPB salt (red), PTSAM salt (blue) pure components and the DES2 (1:3) (green). New peaks observed in the spectrum are encircled orange. δ – bending; ν – stretching. Ref. - [30]. (color).

hydrogen-bonding interactions by the PTSAM and may be due to changes in the water content of the d_6-DMSO solvent.

A critical discussion here is the extent to which the dilution of the DES in DMSO influences the interactions present. However, ^1H-NMR was also done on neat DESs that were not diluted by another solvent. The similarity in Fig. S2 and Fig. S4 reveals that dilution by d_6-DMSO did not interfere much with the DESs, and DESs integrity was preserved, validating the NMR study undertaken here.

Although a certain missing peak was observed when comparing neat (Fig. S4(b)) and solvent-diluted, DES2 (F-6.16 ppm, Fig S2(e)). This peak may simply be a water dependent peak. There is plausible exchange within the sulfonic acid-H and bound water, and the peak might represent the sulfonic acid-H + residual water. In the neat systems, this will shift substantially (wandering peak) or may even broaden out to be challenging to see (but being picked up by MestReNova), the latter being the case observed for DES2.

3.5. Thermal decomposition analysis

Knowledge of a solvent's thermal stability is essential to assess its viability for applications that require heating. Since many DESs decompose before reaching the boiling point of the individual components, the highest operating limit of the DESs is characterized by the degradation temperature (T_{deg}), while the lowest operating limit is characterized by the melting point (T_m). T_{deg} can be approximated by T_{onset}, the lowest temperature where evidence of degradation is observed during a TGA experiment. Table 2 shows the specific temperature ranges and related mass changes seen during the experiment. TGA plots for both DESs are demonstrated in Fig. S3.

Table 2
Data from TGA analysis for the DESs.

DES	Temperature (K)	Mass change (%)	T_{onset} (K)
DES1	298.15 -403.15	1.75	373.45
	403.15–773.15	47.63	558.75
DES2	298.15 -408.15	9.81	362.95
	408.15–773.15	51.81	644.85

In the TGA analysis of DES1, the initial loss of 1.71 mass % is attributed to the partial loss of water (monohydrate content) from the DES. Further mass loss begins around 558.15 K (285 °C, T_{onset}), which may be attributed to the evaporation of PTSAM, as has been reported previously [35], and would include the loss of residual, tightly bound water. For DES2, in the first stage (298.15 K - 408.15 K), 9.81% mass loss is observed and attributed to the complete loss of water from PTSAM. Additionally, Br- is more nucleophilic than HSO_4^- so it is possible this may have catalyzed a partial degradation of either the phosphonium (e.g. nucleophilic attack to form bromobenzene which then leaves) or PTSAM. Further mass loss is observed beginning at 644.15 K (371.7 °C, T_{onset}), which expected to be the complete loss of PTSAM [35,36]. These results highlight that these DES are likely to be stable to temperatures of up to 523 K which is safely lower than degradation onset temperature (T_{onset}) for both DES, although it must be noted that these TGA

experiments involved relatively rapid temperature ramps meaning this range of stability is based on the short term rather than long term stability at the temperatures tested.

3.6. Density, viscosity and conductivity

Mass density, viscosity, and electrical conductivity can provide insight into how ionic mobility changes with fluidity ($1/\eta$). Table 3 summarizes the density, viscosity and conductivity of the two DESs as a function of temperature.

The density of both DESs falls in the conventional range of 1–1.3 g cm^{-3} and shows the expected inverse proportionality with temperature, satisfying the equation $\rho = \left(a - \frac{b}{T}\right)$, where T is in Kelvin [37]. Values for the equation constants a and b are 1.43 g cm^{-3} and 851 g K cm^{-3} for DES1 (R^2=0.9897) and 1.62 g cm^{-3} and 974 g K cm^{-3} for DES2 (R^2=0.9899), respectively.

As a result of its correlation to mass and heat transfer, as well as the movement of electrons within a liquid, viscosity plays a significant role for many applications, particularly as a solvent for chemical reactions. Fig. 4(a) depicts the change in dynamic viscosity (η) with temperature for the two DESs. The viscosity of the DESs can be fitted according to the linearized equation; $ln(\eta) = ln(\eta_0) + \frac{E_\eta}{RT}$, where R is the gas constant (J/mol K), E_η is the energy for activation of viscous flow (J/mol), η is the viscosity (Pa s), and η_0 is the viscosity constant (Pa s). The fits to this equation and the corresponding fitted parameters are depicted in Fig. 4 (a).

The viscosity of DES1 and DES2, at 343.15 K are 0.124 Pa s and 0.288 Pa s, respectively. This indicates both fluids are highly viscous as they possess higher viscosity than solvents such as water (0.001 Pa s, 298.15 K), conventional DESs: reline (0.119 Pa s, 323.15 K) [38], ethaline (0.04 Pa s, 298.15 K) and glyceline (0.30 Pa s, 298.15 K) even at a higher measured temperature [37]. The high viscosity of the DESs is likely due to the components' highly associated nature, including the formation of extensive hydrogen bond networks, which would reduce the mobility of species within the DESs [39]. This association between species leads to forming small void spaces within the fluid, which, when combined with the relatively large size of the DES constituents, contribute to the high viscosity observed. In Fig. 4(a), it was observed that with increasing temperature the DESs become less viscous, which is beneficial for high temperature applications.

One of the many potential uses of DESs is in electrochemical applications. Due to their relatively high viscosity, the two DESs display low electrical conductivities at ambient temperatures. In Fig. 4(b), variations in the electric conductivity of the studied DESs as a function of temperature are shown. Electrical conductivity tends to increase with increasing temperature due to the reduction in viscosity, leading to more mobile charge carriers. Between samples, conductivity depends on these charge carriers' inherent nature and mobility. Fig. 4(b) demonstrates that conductivity is higher for the less viscous DES1. This is consistent with a finding that ammonium-based DESs typically exhibit higher electrical conductivity than similar phosphonium-based DESs [40]. The DES conductivities fit the Arrhenius-like equation used to fit the viscosity values, as has been indicated for other related systems in the literature [41,42]. The fitted results are presented in Fig. 4(b).

It has been proposed that a Walden plot can be used to identify the ionicity of a fluid (i.e. the extent it behaves as a traditional electrolyte). These graphs are generated by plotting fluidity against molar conductivity on a log-log scale according to Eq. (2).

$$\Lambda_m \eta = k \tag{2}$$

where Λ_m (S cm^{-2} mol^{-1}) is the molar conductivity and k is a constant. The variations of log(Λ) vs log(η^{-1}) for DES1 and DES2 are shown in Fig. 5, with other commercial DESs, ILs and 0.01 M KCl presented for comparison. The Walden plot has been used historically as a simple guide to determine whether ions move independently or if they are highly associated since highly associated ions will have proportionally lower molar conductivity for the same fluid viscosity. In contrast, weakly associated ions will have higher conductivities (i.e. be at or above the ideal reference line defined by 0.01 M KCl which is assumed to consist only of independent, solvent-separated ions) [43]. Like the commercial choline-based DESs, DESs in this study are typically close to the ideal line, similar in trend to those of ILs. However, DES2 displays a distinctively different slope compared to the other solvents, with a significant deviation below the KCl line at lower temperatures before meeting the KCl line at elevated temperatures. This can be attributed to the very viscous nature of DES2 in comparison to all other solvents represented in the plot, alongside a significant decrease of viscosity with temperature over the small temperature profile considered. A similar trend has been reported for a DES formed between choline chloride and p-toluenesulfonic acid (1:2) [44].

The behavior of DES2 indicates the ions likely remain highly associated at low temperatures but dissociate at elevated temperatures to form ions that move independently, hence the approach to the ideal line followed by the change in slope as it is reached. On the other hand, DES1 has closer to the ideal behavior throughout. DES2 would be classified as "subionic" at low temperatures due to its significant deviation below the ideal line [45,46]. However, at higher temperatures, both the DESs tend to reach the ideal line and, based on the trend, would likely cross above it at higher temperatures meaning at these temperatures, they behave in an "ionic" nature, akin to a traditional electrolyte.

There has been some recent criticism of the use of Walden plots to assess ionicity, suggesting that these plots do not always account for the molecular-level interactions present. Nonetheless, Walden plots yield qualitative evidence on the average mobility of ions in solution and thus reflect the fraction of free charge carriers to some extent. It also suggests a potentially different mechanism for the mobility of charge carriers in the two DESs under investigation here. However, the significant deviation for DES2 may be due to the temperature being close to the melting point of the liquid, a situation which can lead to the decoupling of mass and momentum transfer in the fluid [49].

3.7. Self-diffusion study

Given some controversy over the Walden plot's use to assess ion mobility in ILs and DESs, the diffusion of individual components was investigated by NMR. Fig. S4 shows the ^1H-NMR spectra of both the studied DESs at 298 K for DES1 and 340 K for DES2. For DES1, there was no overlapping of component signals, while in the case of DES2, there was considerable overlap of the aromatic signals. Nonetheless, the cation of each salt and PTSAM had at least one distinguishable signal enabling their diffusion to be monitored using this technique, as shown in Fig. S4.

Fig. 6(a) and (b) display the self-diffusion coefficients of the cation and PTSAM for each DES (log scale) against the inverse of absolute temperature, where straight lines (dotted and dashed) are fitted trend lines for each respective series. The diffusion coefficients for DES1 are uniformly larger

Table 3
Mass density (ρ), dynamic viscosity (η), and electrical conductivity (κ) of synthesized DESs at different temperatures.

Temperature (K)	ρ (g/cm^3), DES1	ρ (g/cm^3), DES2	η (Pa s), DES1	η (Pa s), DES2	κ (μS/cm), DES1	κ (μS/cm), DES2
323.15	1.157	1.308[a]	0.458		320	
333.15	1.152	1.300[a]	0.227		626	
343.15	1.142	1.288	0.124	0.288	1086	208
353.15	1.131	1.277	0.077	0.228	1678	405
363.15	1.125	1.271	0.055	0.181	2955	717

[a] DES2 is solid at this temperature, so the value is calculated from the fitted density equation.

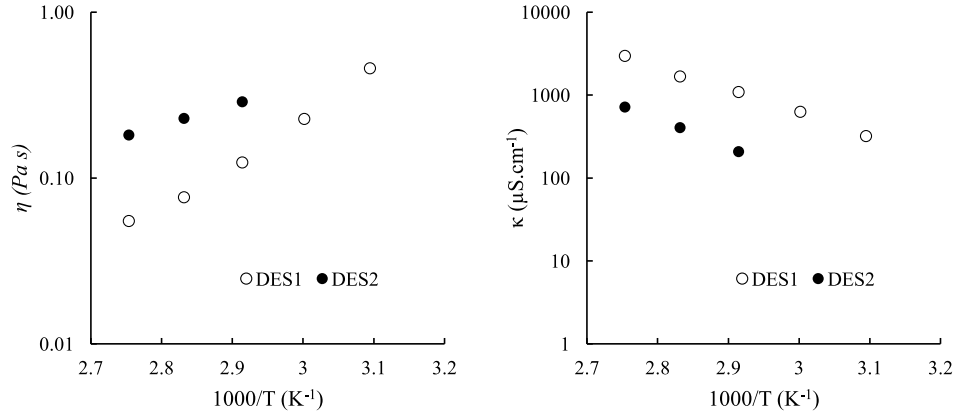

	η_0 (Pa s)	E_η/R (K)	R^2
DES1	6.99E-09	5.74	0.9841
DES2	78.5E-05	2.81	0.9992

(a)

	κ_0 (μS/cm)	E_κ/R (K)	R^2
DES1	2.02E-10	-5.77	0.9835
DES2	7.38E-12	-8.35	0.9981

(b)

Fig. 4. Plots of linearized, (a) Dynamic viscosity (η), and (b) Electrical conductivity (κ) vs inverse of temperature for DESs. Values of fitted parameters are tabulated below respective plots. Negative signs for E_k/R values indicate a negative slope and do not imply negative activation energy.

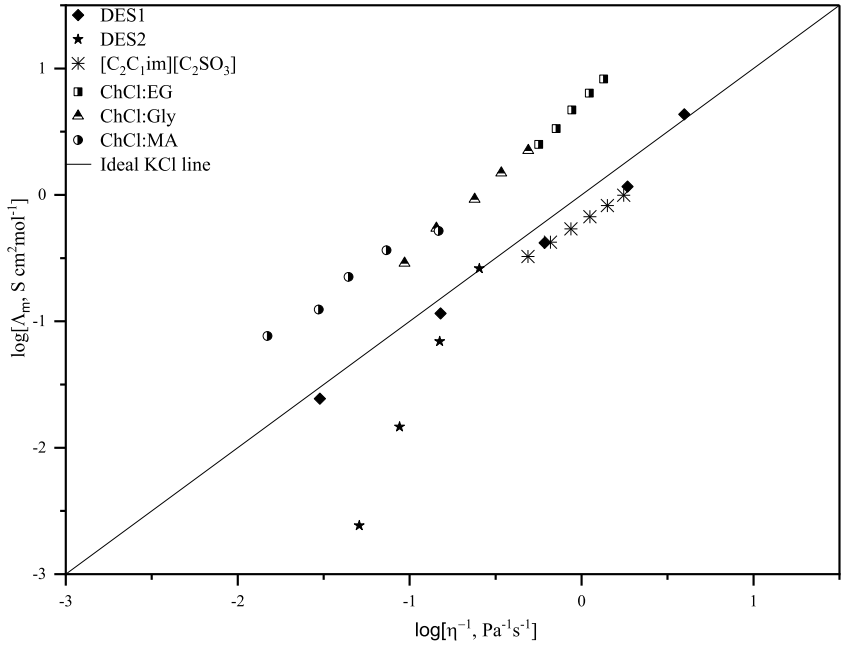

Fig. 5. Walden plot showing ionic mobility vs the fluidity ($1/\eta$) for KCl (aqueous), IL and choline chloride-based commercial DESs at a temperature range of 323.15–363.15 K. Data for ionic liquid: 1-ethyl-3-methylimidazolium ethylsulfonate $[C_2C_1im][C_2SO_3]$ [47] and for choline chloride (ChCl) based DESs [48].

than for DES2, consistent with the lower viscosity of this DES, as has been discussed earlier. Both of the plots in Fig. 6 show good fits to the Arrhenius equation. The activation energies for TBA^+, PTSAM (in DES1), TPP^+, and PTSAM (in DES2) are 106.3 (±0.5) kJ/mol, 107.3 (±0.6) kJ/mol, 76 (±1) kJ/mol, and 62 (±3) kJ/mol, respectively. Higher values indicate a larger activation energy of diffusion. Error for activation energies only accounts for the standard deviation of the fit, excluding uncertainty error in the estimation of D_s.

Since both the DESs have PTSAM as a common HBD, it is plausible to assume that the behavioral differences regarding their molecular motion are influenced more by the respective HBAs. A key result is that the DES1 components PTSAM and TBA^+ diffuse at the same rate, whereas the DES2 components diffuse at different rates, with PTSAM having a higher rate of diffusion. This suggests that DES1 is entirely associated with the PTSAM forming a 2:1 complex, whereas DES2 is more of a solution of TPPB in PTSAM, with the PTSAM able to move independently of the rest of the DES. It is possible that PTSAM forms a similar 1:2 complex with the anion in DES2 as in DES1, but due to the higher proportion of PTSAM in this DES (1:3), this leads to the presence of PTSAM not engaging in hydrogen bonding interactions with the anion, accounting for the PTSAM diffusivity being greater than the cation for DES2. It is reasonable here to foster the consideration that bisulphate anion is interacting with PTSAM. Hence it is proposed here that the equilibrium structure of DES1 and DES2, follows conventional DESs, where a complex anion

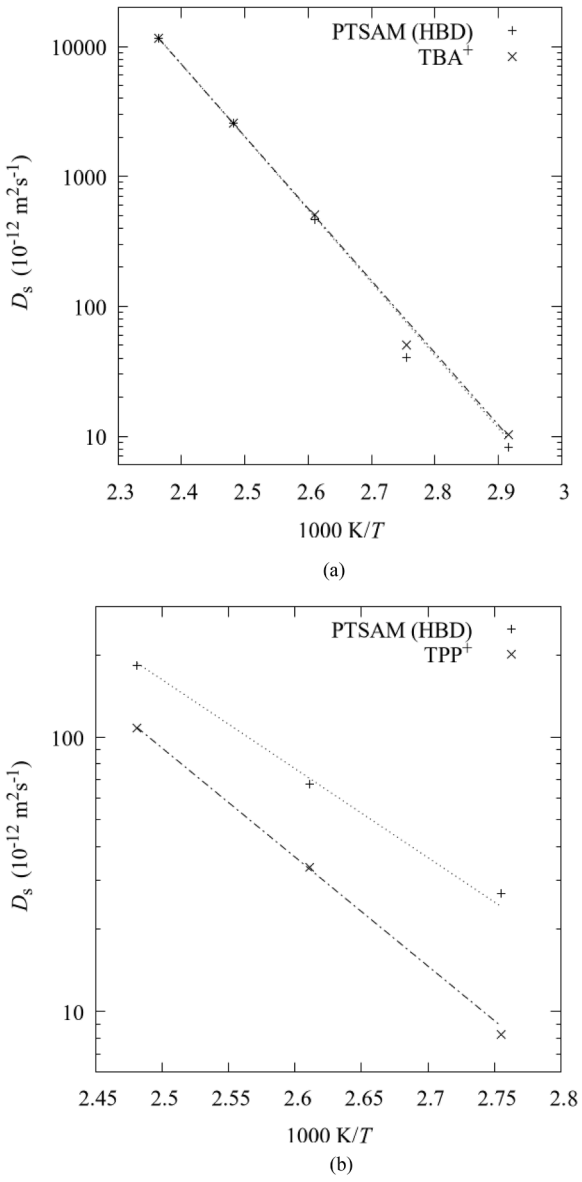

Fig. 6. Arrhenius plots of the self-diffusion coefficients for the respective cation species and common HBD in synthesized DESs; (a) DES1 (343 – 423 K), (b) DES2 (363 – 403 K).

between anion of HBA and HBD is formed due to delocalization of charge [50]; where in case of DES1 more profound interactions exists in the complex anion formed.

In Fig. 7, the diffusion coefficient (D_s) is plotted against T/η in accordance with the Stokes-Einstein equation, Eq. (3) [51], which relates the hydrodynamic radius (r) and D_s.

$$D_s = \frac{k_b * T}{6\pi\eta r} \tag{3}$$

Where k_b is the Boltzmann constant ($1.380649\times10^{-23}\,m^2kgs^{-2}K^{-1}$).

The slope of the curves in Fig. 7 should be proportional to $1/r$, suggesting that DES2 would have the larger ionic radii. However, it is also observed that neither of the Stokes-Einstein curves would go through the origin, even in a linearized plot instead log-log plot shown here, implying the inapplicability of the Stokes-Einstein model for these DESs.

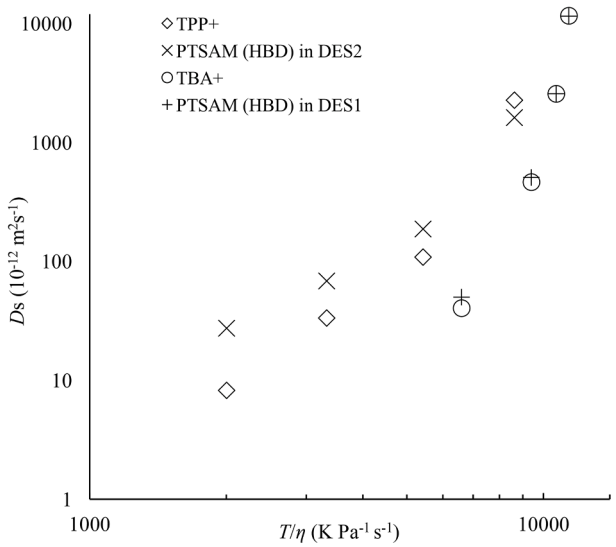

Fig. 7. Plot of D_s vs T/η for the DES1 and DES2 in 363.15 - 423.15 K thermal range. Temperature for datasets increases from left to right.

3.8. Hammett acidity measurements

The acidity of DESs was measured using a Hammett acidity (H_0) method. These DESs could not be measured neat due to their viscosity and melting point, hence they were measured at varied concentrations in an aqueous solution, as previously described for similar DES [44]. Additionally, water has a dielectric constant, recommended for solvents used in H_0 evaluation. This also facilitated the comparison with related p-toluenesulfonic acid studies. These measurements were performed at increasing concentrations to determine the effect of concentration on H_0. From this, clear concentration-dependent trends emerge which give insight into the likely behavior of the Hammett acidity in the neat mixture as they reflect the effect of the increasing association of the DES. Fig. 8 shows the effect of concentration on H_0 for DES1, DES2 and PTSAM. The plot shows that the sequence of acidities among the three species is DES1 ≈ PTSAM > DES2. This highlights the influence of the salt component of the DES, with TBAHS not strongly influencing the acidity of the PTSAM. In contrast, TPPB leads to notably lower acidity compared to pure PTSAM at higher concentrations. The origin of this behavior is not clear but may be due to hydrogen bonding interactions between PTSAM and the Br^- anion of TPPB reducing the acidity of the PTSAM, whereas the $[HSO_4]^-$ anion in TBAHS is amphoteric, which may help offset any reduction in acidity due to hydrogen bonding

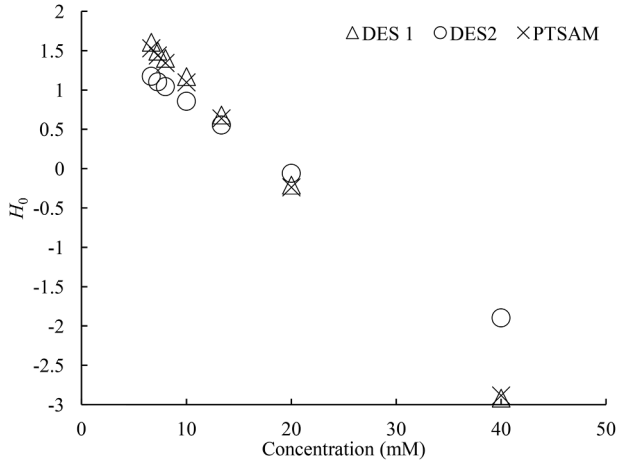

Fig. 8. Hammett acidity for studied DESs at different aqueous concentrations.

effects. In the study mentioned above [44], the H_0 of choline chloride and PTSAM-based DES, the H_0 of 1:2 choline chloride: PTSAM was reported to be 0.87 at a 40 mM concentration. In comparison, DES1 and DES2 have much lower H_0 values of -2.91 and -1.89, respectively. This highlights the influence of salt on the acidity of these PTSAM DESs. To validate this fact, the acidity of a DES composed of allyltriphenyl phosphonium bromide (ATPPB) and PTSAM (1:3) was also measured, with a value of $H_0 = 0.42$ at 40 mM concentration. Compared with DES2, the tetraphenylphosphonium (TPP^+) cation imparts greater acidity to DES2 compared to the closely related allyltriphenylphosphonium cation. Clearly, the additional phenyl group in place of the aliphatic allyl group promotes the acidity of the DES.

Moving on, the same ATPPB-based DES has been shown to catalyze the glycerolysis of oleic acid [13]. It is also noteworthy to mention that while PTSAM is much more acidic than ATPPB-based DES (Fig. 8), it was still inferior to ATPPB-based DES for the previously discussed glycerolysis reaction. As such, it is highly likely that the ATPPB influences this catalytic performance. Since DES1 and DES2 are much more acidic than aforementioned ATPPB-based DES, both DES1 and DES2 may plausibly improve the reaction rate, although this would require further investigation.

4. Conclusions

Two novel acidic DESs were prepared and characterized in this study based on PTSAM as an HBD. The characterization of these DESs included their physical properties such as melting point, density, viscosity and conductivity, with DES2 based on a tetraarylphosphonium salt being more viscous and having a higher melting point than DES1 based on a tetraalkylammonium salt. A Walden plot indicated that DES2 transitions from subionic to an ionic electrolyte with increasing temperature, whereas DES1 is ionic at all explored temperatures. Self-diffusion NMR studies identified that PTSAM and the TBA^+ cation in DES1 diffused at similar rates, whereas the PTSAM diffused faster than the TPP^+ in DES2. Hammett acidity measurements demonstrated that both DESs are more acidic than similar DESs based on choline or allyltriphenylphosphonium cations, with DES1 showing similar acidity to the pure PTSAM. From these findings and the vibrational spectroscopy results, it is interpreted that DES1 acts as a strongly associated hydrogen bond complex between PTSAM and the $[HSO_4]^-$ anion, forming a large complex anionic species. There is some association between PTSAM and Br^- in DES2, as indicated by the IR results, but this seems to be an incomplete association with some free PTSAM present.

Both the DESs showcase good acidity and solvation properties, comparable to ILs that have been proposed as acid catalysts for reactions including transesterification and aldol reactions. These DESs exhibit comparable catalyst properties to these ILs and bring in the beneficial preparation and handling properties of DESs. The study helps to further the scientific knowledge on the properties of acidic DESs and provides an outline for preparing DESs with related properties.

CRediT authorship contribution statement

Kapil Mamtani: Conceptualization, Methodology, Formal analysis, Visualization, Data curation, Investigation, Validation, Writing – original draft. **Sarah J. Stevenson:** Investigation, Formal analysis, Data curation, Writing – review & editing. **Petrik Galvosas:** Investigation, Formal analysis, Visualization, Writing – review & editing, Resources. **Cameron C. Weber:** Validation, Visualization, Resources, Writing – review & editing. **Mohammed.M. Farid:** Supervision, Writing – review & editing, Resources. **Kaveh Shahbaz:** Conceptualization, Supervision, Methodology, Formal analysis, Visualization, Validation, Writing – review & editing, Resources.

Declaration of Competing Interest

The authors declare that they have no known competing financial interests or personal relationships that could have appeared to influence the work reported in this paper.

Data availability

Data will be made available on request.

Acknowledgements

We acknowledge the New Zealand Government through the Ministry of Foreign Affairs and Trade (MFAT) for providing New Zealand Development Scholarships.

Supplementary materials

Supplementary material associated with this article can be found, in the online version, at doi:10.1016/j.molstruc.2023.136378.

References

[1] M. Sert, Catalytic effect of acidic deep eutectic solvents for the conversion of levulinic acid to ethyl levulinate, Renew. Energy 153 (2020) 1155–1162.
[2] Z. Wang, et al., The effect of acidic ternary deep eutectic solvent treatment on native lignin, ACS. Sustain. Chem. Eng 10 (38) (2022) 12569–12579.
[3] M..T.T. Nguyen, et al., Mechanism of friedel–crafts acylation using metal triflate in deep eutectic solvents: an experimental and computational study, ACS. Omega 8 (1) (2023) 271–278.
[4] Q. Li, et al., Coordination of acidic deep eutectic solvent–chromium trichloride catalytic system for efficient synthesis of fructose to 5-hydroxymethylfurfual, Ind. Eng. Chem. Res 59 (39) (2020) 17554–17563.
[5] S. Sarmad, et al., Carbon dioxide capture with ionic liquids and deep eutectic solvents: a new generation of sorbents, ChemSusChem 10 (2) (2017) 324–352.
[6] F. Pena-Pereira, J. Namieśnik, Ionic Liquids and Deep Eutectic Mixtures: Sustainable Solvents for Extraction Processes, ChemSusChem 7 (7) (2014) 1784–1800.
[7] MA Kareem, FS Mjalli, MA Hashim, IM. Alnashef, Phosphonium-based ionic liquids analogues and their physical properties, J.. Chem. Eng. Data 55 (11) (2010) 4632–4637.
[8] MA Kareem, FS Mjalli, MA Hashim, IM. AlNashef, Liquid–liquid equilibria for the ternary system (phosphonium based deep eutectic solvent–benzene–hexane) at different temperatures: A new solvent introduced, Fluid. Phase. Equilib 314 (2012) 52–59.
[9] A Hayyan, M Ali Hashim, FS Mjalli, M Hayyan, IM AlNashef, A novel phosphonium-based deep eutectic catalyst for biodiesel production from industrial low grade crude palm oil, Chem. Eng. Sci 92 (2013) 81–88.
[10] M Hayyan, MA Hashim, MA Al-Saadi, A Hayyan, IM Alnashef, MES Mirghani, Assessment of cytotoxicity and toxicity for phosphonium-based deep eutectic solvents, Chemosp 93 (2) (2013) 455–459.
[11] K Shahbaz, S Baroutian, FS Mjalli, MA Hashim, IM. AlNashef, Densities of ammonium and phosphonium based deep eutectic solvents: prediction using artificial intelligence and group contribution techniques, Thermochim. Acta 527 (2012) 59–66.
[12] T Zhang, K Shahbaz, MM. Farid, Glycerolysis of free fatty acid in vegetable oil deodorizer distillate catalyzed by phosphonium-based deep eutectic solvent, Renew. Energy 160 (2020) 363–373.
[13] ST Williamson, K Shahbaz, FS Mjalli, IM AlNashef, MM. Farid, Application of deep eutectic solvents as catalysts for the esterification of oleic acid with glycerol, Renew. Energy 114 (2017) 480–488.
[14] J Wang, Y Liu, Z Zhou, Y Fu, J. Chang, Epoxidation of soybean oil catalyzed by deep eutectic solvents based on the choline chloride–carboxylic acid bifunctional catalytic system, Ind. Eng. Chem. Res 56 (29) (2017) 8224–8234.
[15] B Tang, KH. Row, Recent developments in deep eutectic solvents in chemical sciences, Monatshefte. für. Chemie. -. Chemical. Monthly 144 (10) (2013) 1427–1454.
[16] K Mamtani, K Shahbaz, MM. Farid, Glycerolysis of free fatty acids: a review, Renew. Sustain. Energy. Rev 137 (2021), 110501.
[17] K Mamtani, K Shahbaz, MM. Farid, Deep eutectic solvents – Versatile chemicals in biodiesel production, Fuel 295 (2021), 120604.
[18] C. Florindo, et al., Quest for green-solvent design: from hydrophilic to hydrophobic (Deep) eutectic solvents, ChemSusChem 12 (8) (2019) 1549–1559.
[19] C D'Agostino, RC Harris, AP Abbott, LF Gladden, MD. Mantle, Molecular motion and ion diffusion in choline chloride based deep eutectic solvents studied by 1H pulsed field gradient NMR spectroscopy, Phys. Chem. Chem. Physs 13 (48) (2011) 21383–21391.

[20] LP Hammett, AJ. Deyrup, A series of simple basic indicators. I. The acidity functions of mixtures of sulfuric and perchloric acids with water1, J. Am. Chem. Soc 54 (7) (1932) 2721–2739.
[21] A Zhu, Q Li, L Li, J. Wang, One-pot synthesis of 3,4-dihydro-2(H)-pyrimidinones catalyzed by reusable acidic choline-based ionic liquids, Catal. Lett 143 (5) (2013) 463–468.
[22] H Ghaedi, M Ayoub, S Sufian, AM Shariff, B Lal, CD. Wilfred, Density and refractive index measurements of transition-temperature mixture (deep eutectic analogues) based on potassium carbonate with dual hydrogen bond donors for CO2 capture, J. Chem. Thermodyn 118 (2018) 147–158.
[23] CR Ashworth, RP Matthews, T Welton, PA. Hunt, Doubly ionic hydrogen bond interactions within the choline chloride–urea deep eutectic solvent, Phys. Chem. Chem. Phys. 18 (27) (2016) 18145–18160.
[24] A Alhadid, L Mokrushina, M. Minceva, Formation of glassy phases and polymorphism in deep eutectic solvents, J. Mole. Liquids 314 (2020), 113667.
[25] KA Omar, R. Sadeghi, Novel benzilic acid-based deep-eutectic-solvents: Preparation and physicochemical properties determination, Fluid. Phase. Equilib 522 (2020), 112752.
[26] M Hayyan, T Aissaoui, MA Hashim, MA AlSaadi, A. Hayyan, Triethylene glycol based deep eutectic solvents and their physical properties, J. Taiwan. Inst. Chem. Eng 50 (2015) 24–30.
[27] J Joseph, ED. Jemmis, Red-, Blue-, or No-Shift in Hydrogen Bonds: A Unified Explanation, J. Am. Chem. Soc 129 (15) (2007) 4620–4632.
[28] H Wang, S Liu, Y Zhao, J Wang, Z. Yu, Insights into the Hydrogen Bond Interactions in Deep Eutectic Solvents Composed of Choline Chloride and Polyols, ACS. Sustain. Chem. Eng 7 (8) (2019) 7760–7767.
[29] SD Muzio, O Russina, D Mastrippolito, P Benassi, L Rossi, A Paolone, et al., Mixtures of choline chloride and tetrabutylammonium bromide with imidazole as examples of deep eutectic solvents: their structure by theoretical and experimental investigation, J. Mole.. Liq. 352 (2022), 118427.
[30] PJ. Larkin, Illustrated IR and raman spectra demonstrating important functional groups, Infrared. Raman. Spectrosc. Princip. Spectral. Interpret (2011).
[31] KI Hadjiivanov, DA Panayotov, MY Mihaylov, EZ Ivanova, KK Chakarova, SM Andonova, et al., Power of infrared and raman spectroscopies to characterize metal-organic frameworks and investigate their interaction with guest molecules, Chem. Rev 121 (3) (2021) 1286–1424.
[32] Spectral Database for Organic Compounds SDBS. National Institute of Advanced Industrial Science and Technology.
[33] S Scheiner, Y Gu, T. Kar, Evaluation of the H-bonding properties of CH···O interactions based upon NMR spectra, J. Mole. Struct. Theochem. 500 (1) (2000) 441–452.
[34] MK Hadj-Kali, S Mulyono, HF Hizaddin, I Wazeer, L El-Blidi, E Ali, et al., Removal of thiophene from mixtures with n-heptane by selective extraction using deep eutectic solvents, Ind. Eng. Chem. Res 55 (30) (2016) 8415–8423.
[35] MA Zolfigol, V Khakyzadeh, AR Moosavi-Zare, G Chehardoli, F Derakhshan-Panah, A Zare, et al., Novel ionic liquid 1,3-disulfonic acid imidazolium hydrogen sulfate {[Dsim] HSO4} efficiently catalyzed N-boc protection of amines, Sci. Iranica 19 (6) (2012) 1584–1590.
[36] HR Shaterian, M Ghashang, M. Feyzi, Silica sulfuric acid as an efficient catalyst for the preparation of 2H-indazolo[2,1-b]phthalazine-triones, Appl. Catal. A. Gen 345 (2) (2008) 128–133.
[37] Marcus Y. Deep Eutectic Solvents. 2019.
[38] F Chemat, H Anjum, AM Shariff, P Kumar, T. Murugesan, Thermal and physical properties of (Choline chloride+urea+l-arginine) deep eutectic solvents, J. Mole. Liq 218 (2016) 301–308.
[39] Q Zhang, K De Oliveira Vigier, S Royer, F. Jérôme, Deep eutectic solvents: syntheses, properties and applications, Chem. Soc. Rev 41 (21) (2012) 7108–7146.
[40] I Wazeer, IM AlNashef, AA Al-Zahrani, Hadj.Kali MK, The subtle but substantial distinction between ammonium- and phosphonium-based deep eutectic solvents, J. Mole. Liq 332 (2021), 115838.
[41] FSG Bagh, K Shahbaz, FS Mjalli, IM AlNashef, MA. Hashim, Electrical conductivity of ammonium and phosphonium based deep eutectic solvents: Measurements and artificial intelligence-based prediction, Fluid. Phase. Equilib 356 (2013) 30–37.
[42] MK AlOmar, M Hayyan, MA Alsaadi, S Akib, A Hayyan, MA. Hashim, Glycerol-based deep eutectic solvents: Physical properties, J. Mole. Liq 215 (2016) 98–103.
[43] K Ueno, H Tokuda, M. Watanabe, Ionicity in ionic liquids: correlation with ionic structure and physicochemical properties, Phys. Chem. Chem. Phys 12 (8) (2010) 1649–1658.
[44] Y Cui, C Li, J Yin, S Li, Y Jia, M. Bao, Design, synthesis and properties of acidic deep eutectic solvents based on choline chloride, J. Mole. Liq 236 (2017) 338–343.
[45] CA Angell, N Byrne, J.P. Belieres, Parallel developments in aprotic and protic ionic liquids: physical chemistry and applications, Acc. Chem. Res 40 (11) (2007) 1228–1236.
[46] J.P Belieres, CA. Angell, Protic ionic liquids: preparation, characterization, and proton free energy level representation, J. Phys. Chem. B 111 (18) (2007) 4926–4937.
[47] FS Oliveira, AB Pereiro, JMM Araújo, CES Bernardes, JN Canongia Lopes, S Todorovic, et al., High ionicity ionic liquids (HIILs): comparing the effect of ethylsulfonate and ethylsulfate anions, Phys. Chem. Chem. Phys 15 (41) (2013) 18138–18147.
[48] Y Wang, W Chen, Q Zhao, G Jin, Z Xue, Y Wang, et al., Ionicity of deep eutectic solvents by Walden plot and pulsed field gradient nuclear magnetic resonance (PFG-NMR), Phys. Chem. Chem. Phys 22 (44) (2020) 25760–25768.
[49] KR. Harris, On the use of the angell–walden equation to determine the “ionicity” of molten salts and ionic liquids, J. Phys. Chem. B 123 (32) (2019) 7014–7023.
[50] AP Abbott, RC Harris, KS. Ryder, Application of hole theory to define ionic liquids by their transport properties, J. Phys. Chem. B 111 (18) (2007) 4910–4913.
[51] A. Einstein, Uber Die Von Der Molekularkinetischen Theorie Der Warme Geforderte Bewegung von in Ruhenden Flussigkeiten Suspendierten Teilchen (English translation: On the Movement of Small Particles Suspended in a Stationary Liquid Demanded by the Molecular-Kinetic Theory of Heat). Investigations on the Theory of the Brownian Movement, Dover, 1905.